Bull Volcanol (2005) 67:634–647
DOI 10.1007/s00445-004-0399-x

RESEARCH ARTICLE

Scott K. Rowland · Harold Garbeil · Andrew J. L. Harris

Lengths and hazards from channel-fed lava flows on Mauna Loa, Hawai'i, determined from thermal and downslope modeling with FLOWGO

Received: 22 September 2003 / Accepted: 18 October 2004 / Published online: 18 February 2005

Abstract Using the FLOWGO thermo-rheological model we have determined cooling-limited lengths of channel-fed (i.e. 'a'ā) lava flows from Mauna Loa. We set up the program to run autonomously, starting lava flows from every 4th line and sample in a 30-m spatial-resolution SRTM DEM within regions corresponding to the NE and SW rift zones and the N flank of the volcano. We consider that each model run represents an effective effusion rate, which for an actual flow coincides with it reaching 90% of its total length. We ran the model at effective effusion rates ranging from 1 to 1,000 $m^3 s^{-1}$, and determined the cooling-limited channel length for each. Keeping in mind that most flows extend 1–2 km beyond the end of their well-developed channels and that our results are non-probabilistic in that they give all potential vent sites an equal likelihood to erupt, lava coverage results include the following: SW rift zone flows threaten almost all of Mauna Loa's SW flanks, even at effective effusion rates as low as 50 $m^3 s^{-1}$ (the average effective effusion rate for SW rift zone eruptions since 1843 is close to 400 $m^3 s^{-1}$). N flank eruptions, although rare in the recent geologic record, have the potential to threaten much of the coastline S of Keauhou with effective effusion rates of 50–100 $m^3 s^{-1}$, and the coast near Anaeho'omalu if effective effusion rates are 400–500 $m^3 s^{-1}$ (the 1859 'a'ā flow reached this coast with an effective effusion rate of ~400 $m^3 s^{-1}$). If the NE rift zone continues to be active only at elevations >2,500 m, in order for a channel-fed flow to reach Hilo the effective effusion rate needs to be ≥400 $m^3 s^{-1}$ (the 1984 flow by comparison, had an effective effusion rate of 200 $m^3 s^{-1}$). Hilo could be threatened by NE rift zone channel-fed flows with lower effective effusion rates but only if they issue from vents at ~2,000 m or lower. Populated areas on Mauna Loa's SE flanks (e.g. Pāhala), could be threatened by SW rift zone eruptions with effective effusion rates of ~100 $m^3 s^{-1}$.

Keywords Mauna Loa · Effusion rate · Channel-fed · Hazard · DEM · SRTM

Editorial responsibility: J Donnelly-Nolan

S. K. Rowland (✉) · H. Garbeil · A. J. L. Harris
Hawai'i Institute of Geophysics and Planetology,
University of Hawai'i at Mānoa,
1680 East-West Road, Honolulu, HI, 96822, USA
e-mail: scott@hawaii.edu

Introduction

The lava flow hazard on the flanks of Mauna Loa is a great concern to State and County planners and Civil Defense officials because eruptions are frequent and because of the growing population living there. There have been 33 eruptions of Mauna Loa since 1843 (Lockwood and Lipman 1987) and flows from these cover 14% of the subaerial surface (Trusdell 1995). Sixteen of these eruptions resulted in a total of 29 flank lava flows (Lockwood and Lipman 1987; Rowland and Walker 1990), and 23 of these were channel-fed 'a'ā flows with initially rapid flow-front velocities.

Although the population of Hawai'i dropped precipitously after the arrival of Westerners in 1778 because native Hawaiians had no resistance to western diseases (e.g. Diamond 1999), this decline halted in 1875 mainly due to the influx of foreigners. Since then the number of people living in Hawai'i has increased significantly (e.g. Trusdell 1995). United States Census data show a 240% increase in the population of the island of Hawai'i between 1960 and 2000 (a 6% increase/year; Office of Planning 2003a). In some areas of the island the population has increased at an even higher rate. For example, in Hawaiian Ocean View Estates, a subdivision just downhill from the axis of the SW rift zone of Mauna Loa, the population increased by >100% between 1990 and 2000, more than 10%/year (Office of Planning 2003b).

Maps that delineate lava flow hazard zones are based primarily on the frequency of coverage by lava flows, probable locations of future eruptive vents, and on topography that is sufficient to either alter or block flow paths (Guest and Murray 1979; Mullineaux et al. 1987; Heliker 1990; Wright et al. 1992; Wadge et al. 1994; Felpeto et al.

2001). Frequency of lava flow coverage is determined by careful field mapping and age dating, and roughly decreases with distance from concentrations of eruptive vents (e.g., rift zones; Guest and Murray 1979; Mullineaux et al. 1987; Heliker 1990; Wright et al. 1992). Guest and Murray (1979) mapped potential lava coverage on Etna (Sicily) by combining vent concentration data, topographically determined flow paths, and a vent-altitude vs. flow-length relationship from Walker (1974). They also analyzed the topography of Etna to determine which potential vent areas threaten each town on the lower slopes of the volcano.

A more quantitative approach for the same volcano was presented by Wadge et al. (1994). They noted that Etna flows tend either to be narrow and simple (Type A) or wide and complex (Type B; see below). They then determined the probability that a new vent would produce either a Type A or B flow field based on its distance from zones on the volcano that had previously produced these types of flows. They combined these probable vent locations and flow types with a numerical flow model (FLOWFRONT; Young and Wadge 1990) that ran over a Digital Elevation Model (DEM) to produce a probabilistic map of flow inundation.

Similarly, Felpeto et al. (2001) assessed the probability of eruption from particular parts of the rift zone on Lanzarote (Canary Islands) and combined this with downslope paths to map the probability of lava coverage. Both the Guest and Murray (1979) and Felpeto et al. (2001) studies noted that towns occur almost exclusively in areas that are less likely to be covered by lava flows, almost certainly because the population has recognized the inundation patterns.

The above examples started with probable vent locations (based on a number of criteria) and let the resulting lava flows head downhill, deriving coverage frequency statistics from the modeled flows. The detailed probabilistic approach of Kauahikaua et al. (1995) differs in that it utilized measured downslope coverage frequency (in 9-km^2 areas of Mauna Loa). These measured frequencies were combined with DEM-derived catchment basins to predict potential downflow paths. The combination was used to delineate small-scale variations within larger hazard zones (e.g. those of Mullineaux et al. 1987; Heliker 1990; Wright et al. 1992).

In the work presented here we have adopted some of the approaches presented in the previous studies. A major difference is that we employ a thermo-rheological model (FLOWGO; Harris and Rowland 2001) that determines flow length based on starting effusion rate, input rheological and temperature parameters, and the underlying slope. To be a useful tool for flow-coverage determinations we ran the model from multiple potential vent locations at multiple effusion rates. The downslope distance that a flow of a particular effusion rate will reach is thus determined from FLOWGO, and areal coverage resulting from that effusion rate is derived by contouring multiple downslope flow ends produced by multiple model runs over a DEM. The starting points (i.e. vents) of the model runs are based on the locations of existing vents in published geological maps (e.g. Lockwood and Lipman 1987). Our approach is non-probabilistic in that it does not consider past patterns of lava inundation nor do we consider any variation in likelihood of eruptions within our potential vent areas. One advantage to this approach is that we do not require knowledge of lava flow ages to derive the inundation patterns.

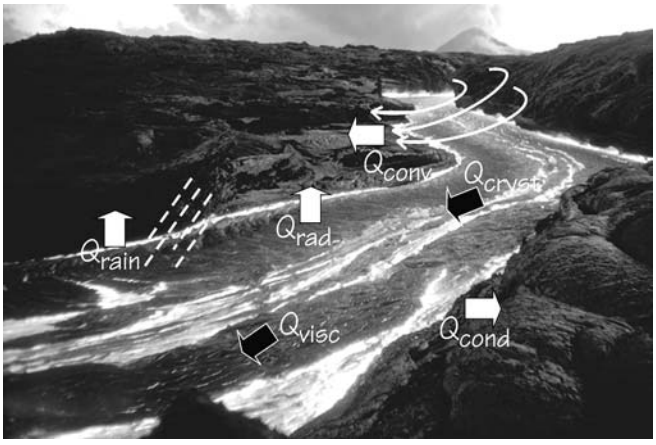

Fig. 1 Diagram showing the heat loss terms (*light arrows*) and heat gain terms (*dark arrows*) in FLOWGO. Q_{rad}=radiative heat loss, Q_{conv}=forced or free convective heat loss, Q_{cond}=conductive heat loss (to levees and base), Q_{rain}=heat lost due to rain (almost always negligible), Q_{cryst}=latent heat of crystallization, Q_{visc}=viscous dissipation

The FLOWGO thermo-rheological model

FLOWGO (Fig. 1; Harris and Rowland 2001) follows an element of lava in an established channel. At the end of each 1-m down-channel step the model calculates all heat-loss and heat-gain terms. These are used to calculate a new flow-core temperature which is in turn used to adjust rheological properties. Finally, the new rheological properties are combined with the underlying slope to determine the velocity with which the element will traverse the next 1-m increment. Flow in the channel is considered to have stopped when any one of the following three conditions are met: (1) velocity becomes zero; (2) the temperature of the flow core reaches the solidus; or (3) the yield strength of the lava is greater than the shear stress at the base of the channel. Note that with FLOWGO we are modeling the length of the well-established channel. Actual lava coverage would include the typically 1 to 2 km-long zone of sheared and dispersed flow (Lipman and Banks 1987) that extends beyond the channel.

Harris and Rowland (2001) compared FLOWGO-derived results with flows from Mauna Loa, Kīlauea, and Etna for which vent locations, eruption durations, effusion rates, and channel dimensions were known. Within ranges necessitated by uncertainties in lava properties such as viscosity, yield strength, vesicularity, and density,

FLOWGO-derived channel lengths were within 10% of known channel lengths. In a recent application, Rowland et al. (2003) used FLOWGO to constrain eruption parameters for the otherwise mostly unobserved 1995 Fernandina and 1998 Cerro Azul eruptions in the Galápagos.

Here, with the goal of estimating the potential for lava inundation on Mauna Loa, we use FLOWGO to estimate channel lengths for flows that have not yet occurred. We therefore do not know the starting vent locations other than that they must be within the regions of Mauna Loa where eruptions have occurred previously, specifically the NE and SW rift zones as well as the N flank (e.g. Macdonald et al. 1983; Lockwood and Lipman 1987). Note that for our modeling purposes an intra-caldera eruption is effectively an upper rift-zone eruption with a vent located where the lava spills out of the caldera. We modeled effusion rates (see below) between 1 and 1,000 m^3 s^{-1}, which is within the range observed or measured previously on Mauna Loa (Rowland and Walker 1990). We were not modeling any particular eruption but instead attempting to bracket all probable scenarios to give a general indication of what areas of the volcano have the potential to be inundated by cooling-limited flows of given effusion rates.

For the work presented here, we modified FLOWGO in three major ways to account for the potential range in effusion rate and vent location. The first of these allows the program to determine its own downslope path across a DEM. The second allows effusion rate to be an input rather than derived parameter. The third automatically moves the starting point of the downslope path so that it can encompass all probable eruption sites on the flanks of Mauna Loa. Additionally, since the original FLOWGO paper was published we have made a few minor modifications that improve the basic mechanics of the model (Appendix).

Utilizing a DEM to derive the flow path

We used an interferometric DEM produced by the Shuttle Radar Topography Mission (SRTM; Zebker et al. 1994; Farr et al. 1995). These data were collected in February of 2000. SRTM DEMs of the United States have a spatial resolution of 30 m and a nominal relative vertical accuracy (i.e., within a single image) of 10 m. The data are available via ftp from the following United States Geological Survey website: http://srtm.usgs.gov/data/obtainingdata.html.

Interferometric DEMs are preferable over DEMs derived by interpolation of contours or spot elevations because the interpolation process often produces artifacts on a scale large enough to affect downslope flow paths. On the other hand, radar energy cannot penetrate thick vegetation and in such areas the resulting elevations in an interferometric DEM represent values somewhere within the vegetation canopy rather than the ground (e.g. Imhoff et al. 1986). This means that where there are distinct vegetation height changes, for example at the boundaries of lava flows of very different ages or at the boundary between forested land and cleared land, the resulting "topographic" barriers can have a significant effect on modeled downslope paths. These effects potentially range from nothing to diversion to blockage if the boundaries are respectively parallel to, sub-parallel to, or perpendicular to, the general downslope direction. Away from such boundaries, however, as long as the forest canopy roughly mimics the underlying topography (i.e., the trees are all essentially the same height), this vegetation problem does not have a large effect on deriving downslope paths. We compared our downslope paths to a vegetation map and could not identify any cases where vegetation boundaries caused obvious deviations or barriers. Because our goal was to determine the downslope extent of many channels associated with many effusion rates rather than to model specific flow paths, even if they occurred such deviations would not affect our overall conclusions.

From each starting pixel, the program determines which of the nearest eight pixels produces the maximum downslope gradient. The program then moves to this pixel and repeats the maximum nearest gradient determination, eventually producing a downslope path. If an enclosed depression is encountered, the program fills the depression and then continues on downslope.

Simple, cooling-limited, channel-fed ʻaʻā flows vs. compound, volume-limited, tube-fed pāhoehoe flows

Basaltic eruptions can be typified by two different effusion rate relationships which produce two different types of flow field, most generally termed simple and compound (Walker 1972). Simple flows consist of one to a few individual flow units or branches, are much longer than they are wide (Kilburn and Lopes 1988), and develop during eruptions that have effusion rates that decrease rapidly from an initially high rate (e.g. Wadge 1981). Examples are the 1981 Etna flow (Guest et al. 1987) and most channel-fed ʻaʻā flows in Hawaiʻi (Rowland and Walker 1990), including the 1984 Mauna Loa flows discussed in more detail below. Individual channel-fed ʻaʻā flows from Puʻu ʻŌʻō (Wolfe et al. 1988; Heliker et al. 2001; Heliker and Mattox 2003) show very little variation in width over slopes that vary from near zero to 25° (e.g. Rowland and Garbeil 2000).

A critical factor with respect to lava inundation hazards are the processes that cause a flow to stop. Most channelized lava flows are cooling limited (Guest et al. 1987; Pinkerton and Wilson 1994; Wright et al. 2001), meaning that heat losses cause the lava to lose its ability to flow beyond a particular distance regardless of the duration of supply from the vent. This maximum distance is attained during the early part of the eruption (see below). Simple, cooling-limited flows were termed Type-A flows by Wadge et al. (1994), are what the FLOWGO model was written to consider, and are the subject of the work presented here.

In contrast, compound flow fields consist of innumerable small flow units, typically have low length:width ratios (Kilburn and Lopes 1988), and are produced by eruptions that are dominated by essentially constant but low effusion rates that may last for months or even years. Examples include the 1983 Etna flow (Guest et al. 1987) and most pāhoehoe flows in Hawai‘i (Rowland and Walker 1990). Other than on the near-horizontal coastal plain where they tend to widen, tube-fed pāhoehoe flow fields from Kūpaianaha and Pu‘u ‘Ō‘ō show little variation in width (Heliker et al. 2001; Heliker and Mattox 2003) over slopes ranging from ~1 to 25° (Rowland and Garbeil 2000).

Because compound flows are typically tube-fed and therefore well insulated, they are volume limited (Guest et al. 1987), meaning that they do not stop advancing until supply from the vent ceases. These are the Type-B flows of Wadge et al. (1994). FLOWGO was not originally written to consider volume-limited flows, and below we briefly discuss our mostly unsuccessful attempt to model them.

As noted above, 16 eruptions have produced 29 major flank lava flows on Mauna Loa since 1843. Ten of the 16 eruptions had durations ranging from 5 to 38 days (average=17 days) and produced only cooling-limited, channel-fed ‘a‘ā flows. Four eruptions (1843, 1859, 1880–81, and 1935–36) had durations ranging from 40 to ~300 days (average=178 days) and initially also produced channel-fed ‘a‘ā flows. However, after a couple weeks of producing channel-fed ‘a‘ā, these 4 eruptions switched to producing tube-fed pāhoehoe, and this continued for the rest of their durations. These were termed “paired eruptions” by Rowland and Walker (1990). The 1855-56 eruption lasted ~450 days and the 1899 eruption lasted 21 days. Both were probably also paired eruptions, however, the flow types and eruptive activity are poorly constrained.

Therefore, of the 29 flank lava flows erupted on Mauna Loa since 1843, at least 23 were channel-fed ‘a‘ā. The average flow-front velocity (flow length divided by eruption duration) of these flows ranged from ~30 to >2,000 m h^{-1} (ignoring one poorly constrained flow with an anomalously low value). In only a few cases, eruption accounts allow instantaneous flow-front velocities to be calculated for these ‘a‘ā flows, and these range from ~250 to >9,000 m h^{-1} (Rowland and Walker 1990), but the point during each eruption when these velocities were measured varies. The 1950 SW rift zone eruption (Finch and Macdonald 1950; Macdonald and Finch 1950) produced six ‘a‘ā flows and these include the highest measured flow-front velocities in the entire data set. Three of these flows crossed HWY 11, the only major road in the area both then and now, 12–14 h after starting from the rift zone, and all three eventually entered the ocean.

Over a longer time period, Lockwood and Lipman (1987) point out that although the surface of Mauna Loa is made up of roughly equal amounts of ‘a‘ā (mostly channel-fed) and pāhoehoe (mostly tube-fed), the distribution is not uniform. In particular, the rift zones have been much more likely to produce ‘a‘ā, especially during the past ~750 years. Much of the tube-fed pāhoehoe that helps to even out the overall percentages was produced prior to then by overflows from Moku‘āweoweo (the summit caldera).

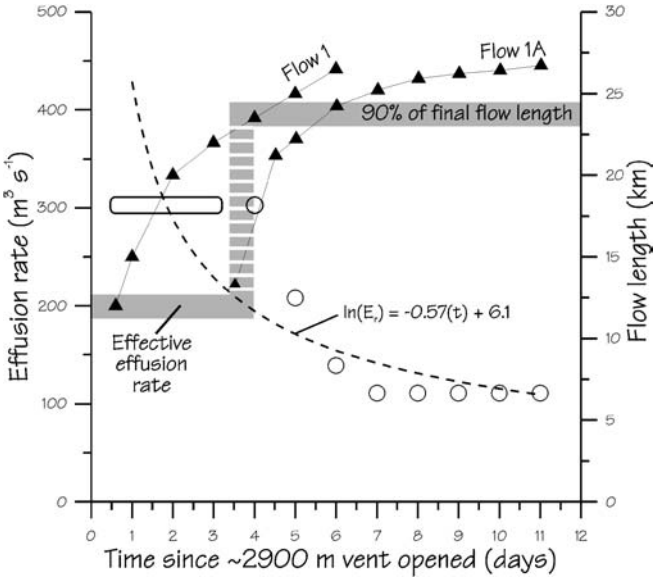

Fig. 2 Graph of effusion rate and flow length vs. time for flows issuing from the ~2,900 m elevation vent during the 1984 eruption. Flow length data (*triangles*) are from Lockwood et al. (1987). Effusion rate data (*circles*) are from Lipman et al. (1985) and Lipman and Banks (1987). The *dashed line* is a best-fit logarithmic fit to the effusion rate data, calculated with the same value (305 m^3 s^{-1}; *open bar*) for days 1, 2, 3, and 4. The 800 m^3 s^{-1} value for the eruption as a whole (see text) was not used in calculating the logarithmic fit. *Grey bands* relate 90% of the flow length with effective effusion rate via *dashed grey band*

Effusion rates and effective effusion rates

A rapidly decreasing effusion rate is common to many basaltic eruptions worldwide (e.g. Wadge 1981; Harris et al. 2000). However, for any one run of FLOWGO in its current configuration, only a single effusion rate can be input. We initially considered modeling either the maximum or the mean effusion rates but the use of either is not reasonable geologically. In the following, using data from the 1984 Mauna Loa eruption, we present the concept of an “effective” effusion rate that corresponds roughly to the maximum length that a cooling-limited flow can reach (Fig. 2).

Descriptions of eruption events as well as flow length data in Fig. 2 are derived from Lockwood et al. (1987). The longest 1984 flows issued from a vent at about 2,900 m elevation on the NE rift zone, and this vent opened on the afternoon of the first day of the eruption (March 25), approximately 12 h after the initial, higher elevation, eruption onset. The first of the two longest flows, Flow 1, had advanced 15, 20, and 22 km away from the vent after 1, 2, and 3 days, respectively (Fig. 2).

On day 3.5 a breach in the channel ~13 km downstream from the vent cut off supply to the lowest ~10 km of Flow 1. Flow 1A issued from this breach and advanced alongside Flow 1. Flow 1A advanced rapidly for about 3 days but slowed considerably once it too had advanced ~25 km from the vent. Another breach, this time ~10 km from the vent, starved Flow 1A and formed Flow 1B. Flow 1B and later channel outbreaks never traveled more than a few km from their origins. Considered together, Flows 1 and 1A extended 26.5 km from the 2,900-m vent and 90% of this distance was attained within the first 4–5 days.

Effusion rates also decreased rapidly during the early part of the eruption (Fig. 2; data from Lipman et al. 1985; Lipman and Banks 1987). At the onset of the overall eruption (i.e., prior to initiation of activity at the ~2,900-m vent), the effusion rate was >800 $m^3 s^{-1}$. For activity from the ~2,900-m vent, which we are concerned with, an effusion rate of slightly more than 300 m^3 s^{-1} was reported for days 1, 2, and 3 based on a volume estimated in the field and divided by time. Lipman and Banks (1987) noted that within the uncertainty of their data, a decay in effusion rate during these three days could not be ruled out. Only by day 4 were instantaneous effusion rate measurements possible. In Fig. 2 we fit a power law decrease to the effusion rate data, and this extrapolates back to a value of around 500 m^3 s^{-1} during the first few hours of activity at the 2,900-m vent.

An inverse relationship can be considered between the effusive driving force and the length of the efficient channel that was able to carry lava to the flow front. Early on, the effusion rate was high but there was no well-established channel and the lava lost considerable energy flowing as unconfined sheets over rough pre-existing ground. As the flow advanced, a channel developed (Lipman and Banks 1987), and allowed more efficient delivery of lava to the flow front. However, by this time the effusion rate had decreased, meaning that the highest effusion rate never coincided with the greatest length of efficient channel. Thus, all the (rapidly decreasing) effusion rates during the first 4–5 days contributed towards getting the flow front 90% of its eventual distance from the vent.

Our challenge, because FLOWGO can only accommodate a single effusion rate, is to select a value within the early effusion rate range that corresponds to this 90% of the flow length. Figure 2 shows that the time associated with the flows reaching 90% of their length corresponds to an effusion rate on the best-fit curve of ~200 m^3 s^{-1}. It is this 200-m^3 s^{-1} effusion rate value that we consider to be the effective effusion rate for the Flow 1/Flow 1A combination. Accordingly, as our results below indicate, when input into FLOWGO, an effusion rate of 200 m^3 s^{-1} produces a flow length corresponding reasonably well with that of Flows 1 and 1A.

Although quantitative data are unavailable for a similar analysis of other Mauna Loa eruptions that produced channel-fed ‘a‘ā flows, the situation probably was qualitatively the same. For example, the 1950 eruption lasted for 23 days, however, after less than 24 h of activity, three separate flows had traveled the ~15 km distance from the rift zone vents to the coastline (Finch and Macdonald 1950; Macdonald and Finch 1950). By days 4 and 5 activity in these and other 1950 flows had decreased and the last 18 days of the eruption were characterized by waning activity both in the lava channels and at the vent, and mostly stagnant flow fronts (Finch and Macdonald 1950).

Effective effusion rates as an input parameter

Because of our desire to model a set range of effective effusion rates, we modified FLOWGO so that effective effusion rate could be an input parameter. Previously in FLOWGO, at-vent channel width and depth are input parameters and these, multiplied by the calculated at-vent mean velocity, produce the effective effusion rate. Note that although the critical variable is the depth of lava flowing in a channel, we use the term channel depth for convenience. Mean velocity in the channel (V_c) is derived from a modified version of the Jeffreys equation (Jeffreys 1925), and adapted here (as described in the Appendix) from Moore (1987):

$$V_c = \left[d^2 \rho_{\text{lava}} g \sin\theta / 3\eta_{\text{lava}}\right]\{1 - (3/2)(\text{YS}_{\text{core}}/\tau_{\text{base-of-channel}}) + (1/2)(\text{YS}_{\text{core}}/\tau_{\text{base-of-channel}})^3\} \quad (1)$$

In Eq. 1 , d is channel depth, ρ_{lava} is lava density, g is gravitational acceleration, θ is the underlying slope, η_{lava} is lava viscosity, YS_{core} is the yield strength of the flow core, and $\tau_{\text{base-of-channel}}$ is the amount of shear stress required to deform the lava at the base of the channel. Mass is conserved in FLOWGO, meaning that the at-vent mean velocity and channel dimensions determine the effective effusion rate for the entire length of the flow.

An iterative approach allows us to treat effective effusion rate as an input parameter. First, once a vent location and a particular effective effusion rate are chosen, FLOWGO determines the steepest downslope path from this location and calculates an average slope along the first 10 DEM pixels of this path. Using this average slope it then iterates on channel dimensions until the desired effective effusion rate is achieved, with the condition that along this uppermost part of the channel, the cross-section is square (depth=width). The square cross section avoids apriori assumptions about channel shape. FLOWGO holds channel depth constant along the entire flow path whereas channel width varies to conserve mass as velocity varies (Harris and Rowland 2001).

Running FLOWGO from multiple starting locations

FLOWGO was developed to model lava flows with known vent locations. In the present study our goal instead is to determine channel lengths for eruptions starting at any geologically reasonable vent location on Mauna Loa (the NE and SW rift zones plus the N flank). For the

purpose of running the FLOWGO program, we define all these vent locations, considered together, as the vent mask.

We developed a routine that runs FLOWGO from multiple pixels within the vent mask. This routine runs the thermo-rheological part of the program down the DEM with a desired effective effusion rate (see above) until the lava stops due to one of the stopping criteria. It then repeats the process at that same pixel for the next effective effusion rate, and so on until all effective effusion rates are run. For each starting pixel the downslope paths for each effective effusion rate differ only in length. After running through all the desired effective effusion rates, the program moves to the next starting point within the mask and repeats the whole process. We tested the sensitivity of the model to subsampling pixel starting locations, and found that the results of using every 4th pixel were similar to those achieved using every pixel.

Using every 4th pixel rather than every pixel reduced the number of FLOWGO runs by a factor of 16 although the total number of starting pixels within the vent mask still exceeded 53,000. For the channelized-flow portion of the current study we used effective effusion rates of 1, 5, 10, 50, 100, and 200, 500, and 1,000 $m^3\ s^{-1}$, resulting in ~424,000 runs of FLOWGO. We could have reduced the number of starting pixels even more by considering only pixels making up the downhill boundary of the potential vent regions (Kauahikaua et al. 1995), although this would have prevented determination of flow paths within the vent regions themselves.

Figure 3 shows a sample of downslope paths for a portion of the SW rift zone. Note that there is a distinct coalescence from many upslope paths to few downslope paths. The pattern is similar to a stream tributary system and gives the mistaken impression that there are areas of the volcano (which get larger downslope) that lava will never cover regardless of vent location. A similar result was noted by Kauahikaua et al. (1995). The whole surface of Mauna Loa has received lava at some time in the past so clearly flows can cover any location that is not topographically protected or does not require travel uphill.

The apparent lack of inundation in particular downslope areas arises for three reasons. The first is related to the quantizing of topography by the DEM. In reality, topography has infinite variability at all scales (e.g. Glaze and Baloga 2003) but it is not possible to duplicate this with a DEM that has a distinct pixel size, which in this case is 30 m. We tested the program over a DEM with 10-m spatial resolution derived from interpolated contours. We found that although the number of potential starting locations and resulting paths increased (with decreased spacing between them), there was still a distinct coalescence of paths downslope, resulting in apparently un-inundated areas. The 10-m spatial resolution DEM was not produced interferometrically so it also allowed us to confirm the lack of vegetation-induced artifacts in the 30-m spatial resolution SRTM DEM (see above). Second, early in most eruptions, vents are linear sources oriented obliquely to the nearby downslope direction. Near such vents, the aggregate surface flow is essentially as wide as the vent is long, but not very far downslope the lava coalesces into one or a few considerably narrower flows. Although we did not attempt to model linear vents, our approach approximates the coverage from such vents by way of the multiple, closely spaced potential point sources. Finally, lava flows have width, meaning that an advancing flow front inundates a swath rather than a line. Even though the exact center of a flow may not pass over a particular location, such a location can very likely be covered by lava. We can produce greater areal coverage by giving our flow paths an arbitrary width based on, for example, the average width of observed Mauna Loa ʻaʻā flows. However, in the current study we are not attempting to model any individual flow paths or even their aggregate distribution and coverage. Instead, our goal is to determine the potential downslope distance that particular effective effusion rate flows can reach. For all calculations, starting (= at-vent) lava properties (rheology, eruption temperature, vesicularity, etc.) are those of the 1984 flow (see Harris and Rowland 2001) because during this most recent Mauna Loa eruption, these properties were measured most accurately.

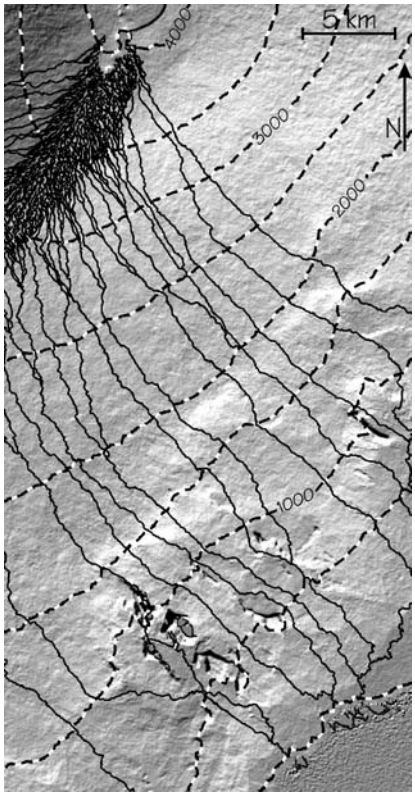

Fig. 3 Flow paths generated by starting at every 4th line and sample in a 30-m spatial resolution SRTM DEM, for a portion of the upper SW rift zone. Elevation contours (*dashed*) are every 500 m. Note that multiple upslope paths merge into an ever-smaller number of downslope paths. If flow width is not taken into account, this leaves large areas of the slope seemingly immune to lava inundation (see text)

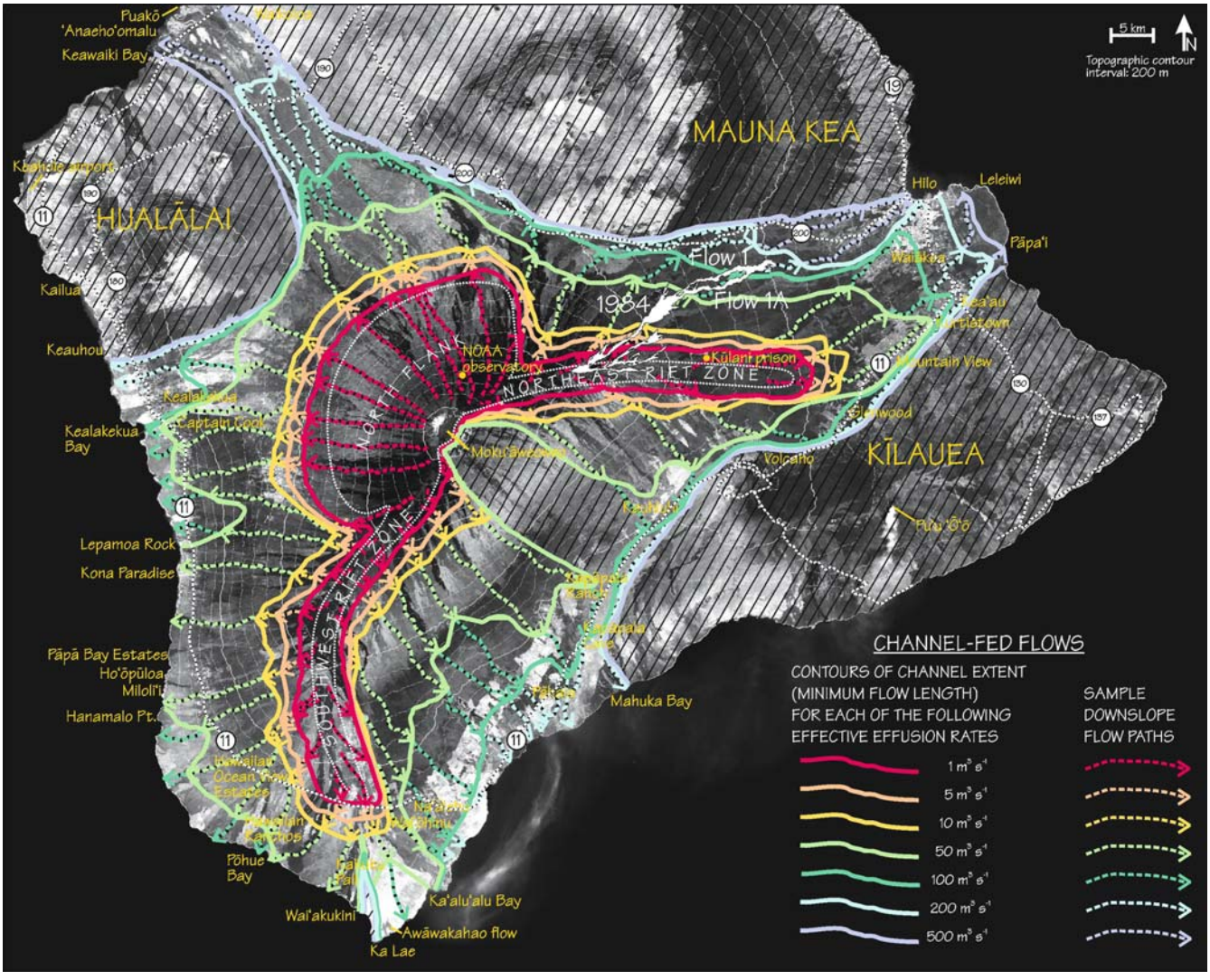

Fig. 4 Results for channel-fed flows superimposed on a portion of a cloud-free Landsat ETM+ image. *White dotted line* highlights the vent mask composed of rift zones and north flank. *Solid color contours* generalize maximum channel lengths for effective effusion rates indicated. A subset of flow paths is included (*dashed colored arrows*). Note the outline of the main 1984 flow, which issued from the ~2,900-m vent (*white*), and that for it to have reached Hilo at its effective effusion rate (200 m^3 s^{-1}), it would have had to erupt from a location 15–20 km farther down-rift (e.g. near Kūlani Prison). *Diagonal ruled lines* indicate areas that are topographically protected from Mauna Loa flows. Highways are shown with *black and white lines* and *circled numbers*

Results

Results for channel-fed flows are shown in Fig. 4, where effective effusion-rate-derived channel length contours are superimposed on a Landsat Enhanced Thematic Mapper+ (ETM+) image (Mouginis-Mark et al. 2003). The contours were drawn by hand to purposely smooth small-scale variations. Recall that FLOWGO determines the distance that lava can travel down an existing channel, meaning that the lengths derived by FLOWGO are those of the established channel. As noted above, this is usually one to a few km shorter than the total flow length (Lipman and Banks 1987). Given our assumptions, the contours presented here are therefore minima with respect to lava inundation. In each effective effusion rate discussion presented below, we move clockwise starting with the W flank of the SW rift zone, moving to vents from the N flank, NE rift zone, and finishing with the E flank of the SW rift zone. The discussion is in order of increasing effective effusion rate and for each of these we discuss only those areas threatened by the increase. In no instance does an increase in effective effusion rate cause an area already threatened by a lower rate to become safe.

Effective effusion rate = 1–10 m^3 s^{-1}

Channels do not extend more than a few km from vent locations and do not pose a threat to any populated locations except for the upper portions of Hawaiian Ocean View Estates near the lower end of the SW rift zone. Because radial vents occur in such a large area of the N

flank (Lockwood and Lipman 1987), much of this region could potentially be covered even by short flows. Note in Fig. 4 that some of the 1-10-m^3 s^{-1} flow paths give the mistaken impression that such flows can be quite long, particularly on the N flank. In reality, many of these flows actually don't make it out of the vent area and these long paths are in fact aggregates of multiple short flows. From the NE rift zone, the NOAA solar observatory and Kūlani Prison could be threatened by such eruptions. There are no human structures at risk from channel-fed, 1–10 m^3 s^{-1} eruptions on the E flank of the SW rift zone.

Note that eruptions at these low effective effusion rates are unlikely to produce channel-fed, cooling-limited flows exclusively. Instead, particularly if the eruptions persist, they are likely to produce lava tubes. As noted above, tube-fed flows are not cooling-limited and therefore not suitable for modeling by FLOWGO (see below).

Effective effusion rate = 50 m^3 s^{-1}

Lava from the lowermost SW rift zone could reach the coast along a short stretch from Wai'akukini to Pōhue Bay, threatening the Hawaiian Ocean View Estates and Hawaiian Ranchos subdivisions in the process. Lava from the mid to upper SW rift zone could reach the coast between Hanamalo Pt. and Lepamoa Rock. Most of the downslope part of this region consists of homes clustered along HWY 11, the only major road on the southern part of the Big Island. Evacuation would be difficult in some cases (e.g. Kona Paradise Subdivision and Pāpā Bay Estates), because homes there are arranged along roads that run up- and down-slope. Similarly, the villages of Hō'ōpuloa and Miloli'i occur at the bottom of generally slope-parallel roads. In all these instances, the only vehicular means of escape other than by boat would be uphill, perhaps towards an oncoming flow. An effective effusion rate of 50-m^3 s^{-1} from the southern part of the N flank could threaten HWY 11 and many of the homes along it in the area south of Captain Cook. Such flows from the northern part of the N flank would reach the saddles between Mauna Loa and Hualālai and between Mauna Loa and Mauna Kea, but these areas are essentially uninhabited. Flows from the upper NE rift zone likewise threaten only uninhabited forest as well as the access road from HWY 200 to the NOAA observatory. From the lowest part of the NE rift zone, however, homes and farms on the NW outskirts of Volcano, Glenwood, Mountain View, and Kurtistown would be threatened by such a 50-m^3 s^{-1} eruption. The SE wall of Moku'āweoweo, the summit caldera, protects the SE flank uphill from the Kīlauea/Mauna Loa boundary between Kauhiuhi and Kapāpala Ranch.

Effective Effusion rate = 100 m^3 s^{-1}

Flows heading west from the SW rift zone and southern portion of the N flank could reach the coast all the way from Wai'akukini to Kealakekua Bay. Flows from the northern portion of the N flank as well as from the upper NE rift zone threaten uninhabited areas but in places could reach HWY 200 (the Saddle Rd.). Flows from the NE rift zone below ~1,800 m elevation, could reach Waiākea and other upslope suburbs of Hilo. S-directed NE rift zone flows could threaten Glenwood and Kea'au in addition to the other nearby towns that are already threatened by 50-m^3 s^{-1} flows. S-directed flows from the uppermost NE rift zone could turn upon reaching the Mauna Loa-Kīlauea boundary and flow SW as far as Kapāpala Cave. The towns of Pāhala, Nā'ālehu, and Wai'ōhinu could be threatened by SE-flowing 100 m^3 s^{-1} flows from the SW rift zone, as would the coastline between Ka'alu'alu Bay and Ka Lae (South Point).

Effective Effusion rate = 200 m^3 s^{-1}

Depending on the vent location, an eruption of this magnitude (which, as noted above, was the effective effusion rate of the 1984 eruption) could affect nearly all locations on Mauna Loa that are not topographically protected. From the SW rift zone, a 200-m^3 s^{-1} flow could reach the W coastline regardless of vent location. This threatens all towns and houses above, along, and below HWY 11 from Ka Lae to Captain Cook. Flows from the southern half of the N flank could reach the coast almost as far north as Keauhou (Keauhou itself is on the flank of Hualālai and therefore protected topographically from Mauna Loa lavas). The 200-m^3 s^{-1} flows from the northern portion of the N flank could threaten a stretch of HWY 190 between Hualālai and Mauna Kea, but otherwise no inhabited areas. Such flows from the upper NE rift zone, as did the 1984 flow, threaten mostly forested areas. An effective effusion rate of 200 m^3 s^{-1} from the NE rift zone below about 2,200 m, however, would threaten most of Hilo and Hilo Bay. If directed S from the mid to lower NE rift zone, such flows could reach all towns along HWY 11 between Kea'au and Volcano. South-directed flows from the uppermost NE rift zone could flow along the Mauna Loa/Kīlauea boundary and reach the coast at Mahuka Bay. East-directed SW rift zone flows could reach the SE coast from Mahuka Bay to Ka Lae and in so doing potentially threaten Pāhala.

Effective Effusion rate = 500 m^3 s^{-1}

Flows could reach essentially the entire coastline of southern Hawai'i Island except for those portions protected topographically by Hualālai, Kīlauea, Moku'āweoweo, and the Kahuku Pali. Flows could also reach the short segment of Mauna Loa coastline north of Hualālai, extending from Keawaiki Bay ~8 km NE to near Puakō. The only region where cooling limitations would prevent flows from extending to the coastline is a short segment southeast of Hilo between Leleiwi and Pāpa'i.

Effective Effusion rate = 1000 m^3 s^{-1}

Flows reach all coastlines of southern Hawai‘i Island except those portions protected topographically by Hualālai, Kīlauea, Moku‘āweoweo, and the Kahuku Pali. The 1,000 m^3 s^{-1} effective effusion rate contour is not shown in Fig. 4.

Tube-fed flows

Although FLOWGO was developed for open channels, we attempted to adapt it to approximate tube-fed flows. This was achieved by forcing the percent of crustal coverage to be 100% along the entire flow length and giving this crust a surface temperature of 60°C. We recognize that fully crusted lava flowing in a channel is not the same as lava flowing in a mechanically stable tube but we were limited by constraints of the model. Additionally, unlike true tube-fed flows, which are volume-limited, the FLOWGO adaptation was cooling-limited.

As would be expected, the complete, cooler crust provides greater insulation and allows each effective effusion rate to carry lava farther than in the partially-crusted cases presented above. For example, our modeled fully-crusted flow with an effective effusion rate of 10 m^3 s^{-1} could extend into much of Hilo or reach all of the SW coastline (partially-crusted flows at 10 m^3 s^{-1} threaten almost no human structures; Fig. 4). However, no 100% crusted model flow with an effective effusion rate of 10 m^3 s^{-1} from the N flank extends to the coastline near Keawaiki Bay, at the NW portion of Mauna Loa, which is contrary to field evidence. As is discussed below, a cooling-limited model with 100% crust considerably underestimates the length of volume-limited tube-fed flows.

Discussion

Our results suggest that in addition to the frequency with which particular regions have been covered by lava and the topography-derived downslope paths of lava flows, consideration of the cooling-limited nature of channel-fed lava flows should be included when assessing potential hazards. The flows that issued from the ~2,900-m vent during the 1984 eruption are included in Fig. 4. Note that the vent is within the NE rift zone part of the vent mask and that the flow front lies between the 100 and 200-m^3 s^{-1} effective effusion rate contours. These contours are maximum downslope channel lengths that would be attained from vents on the downslope edges of the vent masks. Shifting the upslope end of the 1984 flow outline to the downslope edge of the vent mask shifts the flow front nearly to the 200-m^3 s^{-1} contour. As noted in the discussion above, 200 m^3 s^{-1} was defined as the effective effusion rate for the 1984 flow based on its coincidence with the flow reaching 90% of its eventual length (Fig. 2). We are encouraged by this result, particularly recalling that in reality there is considerable variation in modeled flow lengths due to uncertainties in input rheological variables (Harris and Rowland 2001).

Obviously, assessments of potential hazards can also be made more useful by considering prior eruptive behavior of the volcano. However, comparison with pre-1984 eruptions of Mauna Loa is difficult because only mean effusion rates (total flow volume divided by eruption duration) are available. The effective effusion rate for the 1984 flows that issued from the ~2,900-m vent was 200 m^3 s^{-1}, and we note that this is approximately twice the mean effusion rate for the eruption as a whole (~115 m^3 s^{-1}). For the following discussion of pre-1984 channel-fed flows, we will assume that the effective effusion rate is roughly twice the mean effusion rate.

For the 7 channel-fed flows that have been erupted from Mauna Loa‘s NE rift zone since 1843, the mean effusion rates ranged from a poorly constrained 19 m^3 s^{-1} (in 1880) to 157 m^3 s^{-1} (in 1942). The average was ~80 m^3 s^{-1}, which by the relationship noted above corresponds to an effective effusion rate of ~160 m^3 s^{-1}. Additionally, over this same period no NE rift zone eruption has occurred below an elevation of ~2,500 m. Thus although Fig. 4 shows that channelized flows with effective effusion rates between 100 and 200 m^3 s^{-1} could reach much of Hilo, such an occurrence is less likely because it would require a vent at an elevation below ~2,000 m.

Cooling limitations to flow length are also illustrated by the two lowest-elevation NE rift zone eruptions, which occurred in 1852 and 1942 from vents at 2,520 and 2,760 m elevations, respectively (Macdonald et al. 1983). Their mean effusion rates were 105 and 157 m^3 s^{-1}, respectively (Rowland and Walker 1990), corresponding as above to effective effusion rates of ~200 and ~300 m^3 s^{-1}. It is notable that even these, however, did not come closer than ~20 km from Hilo although the 1942 flow in particular caused considerable concern (Macdonald 1943, 1954).

Kauahikaua et al. (1995) suggested that based on topography, Hilo would have been threatened by the 1984 flow had the eruption lasted a longer time. With an important caveat noted below, our results do not agree with this and indicate that the ~2,900-m vent would have required an approximately two-fold higher effective effusion rate for flows to have reached Hilo. Alternatively, had the main 1984 flows issued from an elevation below ~2,000 m, Hilo could have been at risk. The caveat is that if the 1984 eruption had made a transition to the production of continuous, low-effusion-rate tube-fed pāhoehoe after cessation of the high effusion-rate activity (as did the 1843, 1855–56(?), 1859, 1880–81, 1899(?), and 1935–36 eruptions), then we agree with Kauahikaua et al. (1995) that Hilo definitely could have been at risk. Our results, the historic record (e.g. Brigham 1909), and recent geological mapping (Lockwood et al. 1988; Buchanan-Banks 1993; Lockwood 1995) lead to the conclusion that volume-limited, tube-fed pāhoehoe flows pose a much greater threat to Hilo than do cooling-limited, channel-fed ‘a‘ā flows.

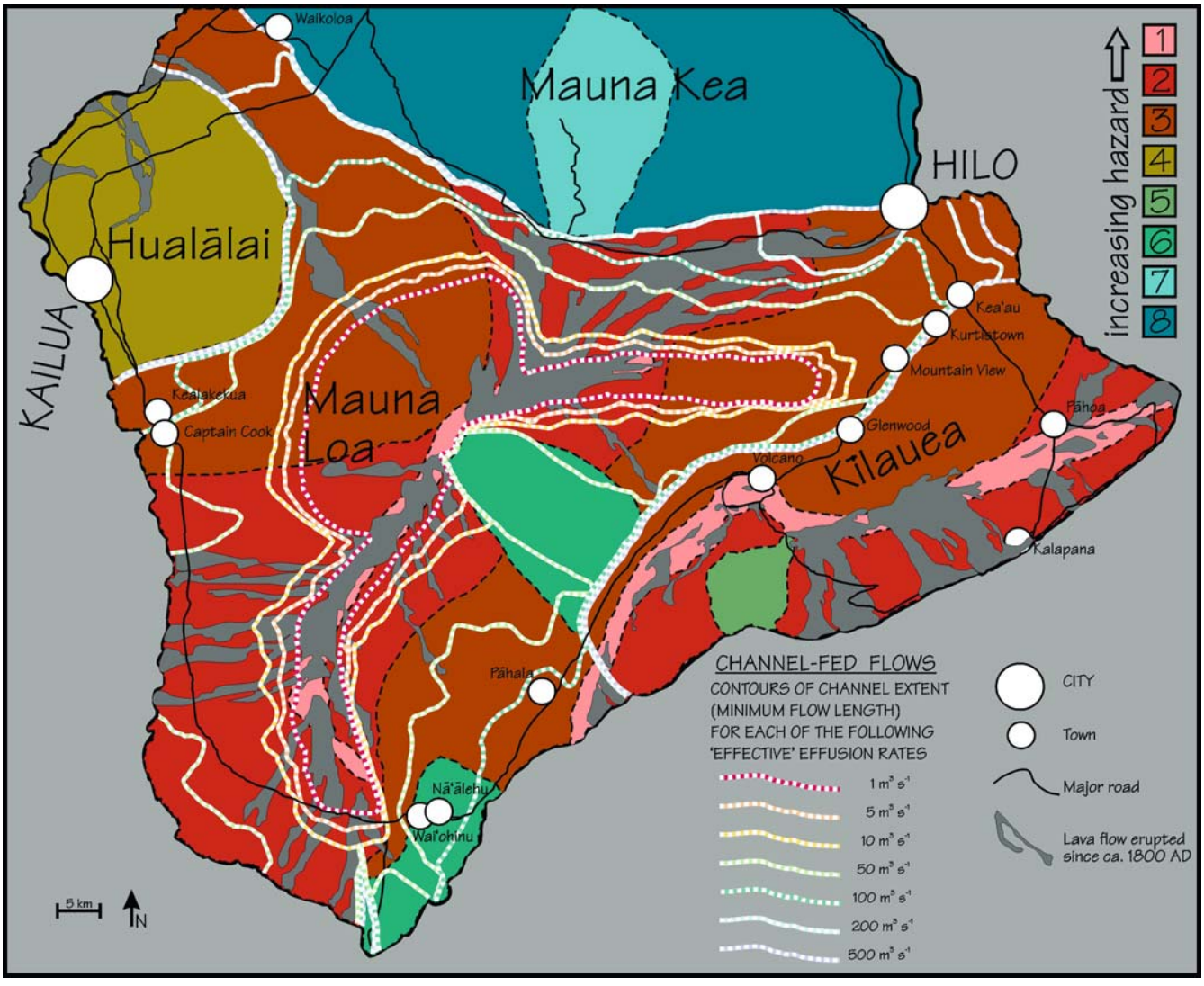

Fig. 5 Lava flow inundation hazard zones for Hawai'i shown with colors indicating increasing hazard (adapted from Heliker 1990; Wright et al. 1992). Superimposed on hazard zones are channel-length contours from Fig. 4 (*dashed color lines*). See text for discussion

The same cannot be said for the communities downslope from the SW rift zone. Here, the average mean effusion rate for the 15 channelized flows emplaced since 1800 is 175 $m^3\ s^{-1}$ (corresponding as above to an effective effusion rate of 350 $m^3\ s^{-1}$). This is actually a minimum value because most of these flows entered the ocean and the submarine volumes are unknown. The typical SW rift zone effective effusion rate since 1800 may therefore be closer to 400 $m^3\ s^{-1}$. Figure 4 shows that such an eruption on the SW rift zone could threaten any location on the S flank of the volcano except the small sliver of topographically protected high ground immediately N of Ka Lae. The risk posed by these flows is compounded by the rapidly increasing rate of development occurring in this region (Trusdell 1995).

Only two eruptions from the N flank have occurred since 1843 (in 1859 and 1877; Macdonald et al. 1983). The 1877 eruption took place offshore within Kealakekua Bay (e.g. Brigham 1909; Moore et al. 1985). The channel-fed 'a'ā portion of the 1859 eruption reached the coastline just south of 'Anaeho'omalu with a mean effusion rate of around 200 $m^3\ s^{-1}$, corresponding to an effective effusion rate of 400 $m^3\ s^{-1}$. This agrees well with our results that show flows with effective effusion rates between 200 and 500 $m^3\ s^{-1}$ reaching this section of coastline (Fig. 4).

The channel-length contours have shapes that are to some extent similar to the boundaries of lava flow hazard zones (Fig. 5; Mullineaux et al. 1987; Heliker 1990; Wright et al. 1992). As noted above, these hazard zones are probabilistic because they are determined by age-dating of flows, recorded activity, and analysis of topography. Comparison of Figs. 4 and 5 shows that along Mauna Loa's rift zones, coverage by channel-fed flows with effective effusion rates $\leq 10\ m^3\ s^{-1}$ roughly corresponds to hazard zone 1 (the greatest hazard). An obvious exception is the downslope end of the NE rift zone. This

is mapped as hazard zone 3 because eruptions have not occurred there recently. Because we included it in our potential vent area, it has the potential for being covered by flows with effective effusion rates ≤ 10 m^3 s^{-1}. The same situation exists in the potential vent area for the N flank flows, which likewise are mapped as hazard zone 3 because of infrequent eruptions. These are the first of a few examples where our non-probabilistic effective effusion rate contours differ from the hazard zone boundaries.

For the W flank downhill from the SW rift zone, the coverage area from flows with effective effusion rates of 50 m^3 s^{-1} corresponds to most of the area that is mapped as hazard zone 2. However, there are a couple of coastal regions where the 50-m^3 s^{-1} contour does not extend to the coastline even though hazard zone 2 does. Much of the N flank, extending as far as the boundary with Hualālai, could be covered by 50 m^3 s^{-1} but again, because of the infrequency of eruptions there this region is mapped as hazard zone 3. For flows from the upper part of the NE rift zone, the 50-m^3 s^{-1} contour does not extend as far as the hazard zone 2 boundary. As we noted above, recent eruptions from this part of the rift zone have had effective effusion rates >50 m^3 s^{-1}. As was the case for lower effective effusion rates, our extending of the potential vent region farther down the NE rift zone than has been active recently causes potential coverage by 50-m^3 s^{-1} flows beyond the hazard zone 2 boundary and well into hazard zone 3. On the E flank of the volcano, the topographic shadowing effect of Moku‘āweoweo‘s SE wall on the 50-m^3 s^{-1} contour corresponds in the hazard map to a region mapped as zone 6. On the E flank downslope from the SW rift zone, the 50-m^3 s^{-1} contour extends 5–10 km farther downslope than the boundary of hazard zone 2. This is because most recent eruptions on the SW rift zone have been W of the topographic axis (limiting the extent of hazard zone 2 on the E flank) whereas our modeling treats the entire axis equally.

The contours for effective effusion rates of 100, 200, and 500 m^3 s^{-1} extend farther and farther into hazard zone 3, the areas that are downslope from the rift zones and N flank vents. Two areas worth noting are mapped as hazard zone 6. The northern one is located on the E flank of Mauna Loa, extending from the SE boundary of Moku‘āweoweo to the Mauna Loa-Kīlauea boundary, and the southern one is near the SE-most point on the island and includes the towns of Nā‘ālehu and Wai‘ōhinu. As noted above, the 50-m^3 s^{-1} effective effusion rate contour matches the N hazard zone 6 relatively closely. Flows with higher effective effusion rates similarly would follow the same downslope paths that define the N and S boundaries of this hazard zone. However, unlike 50-m^3 s^{-1} flows, those with higher effective effusion rates that headed down the N boundary of this zone would follow the saddle between Mauna Loa and Kīlauea all the way to the coastline. Thus, although the region of hazard zone 6 would remain unburied, the contour lines of the higher effective effusion rates are drawn across its SE margin.

The W boundary of the southern hazard zone 6 is the Kahuku Pali, which forms a 100 to 150-m-high barrier to flows coming from the west. The height of Kahuku Pali decreases northward and it disappears just north of HWY. 11. This barrier, combined with the lack of recent flows emanating from the S-most end of the SW rift zone cause the area to be mapped as hazard zone 6. Indeed, much of the surface here consists of the ~25,000-year-old Pāhala ash (e.g. Easton 1987) and flows older than 10,000 years interbedded with Pāhala ash (Lipman and Swenson (1984). However, in all but the part of this hazard zone 6 that is immediately E of the Kahuku Pali, there are no topographic barriers to flows issuing from the lowermost SW rift zone. In fact, the eastern arm of the 1868 flow extends almost to the upslope boundary of this zone and the ~8,000-year-old Awāwakahao flow cuts completely across it and extends to the coastline (Lipman and Swenson 1984). Although the 50-m^3 s^{-1} effective effusion rate contour does not cross into the northern and southern parts of this hazard zone 6, higher effective effusion-rate contours do, and include all but a narrow sliver immediately adjacent to the Kahuku Pali (Figs. 4 and 5).

Note that hazard zone 4 is all of Hualālai and therefore topographically protected from Mauna Loa flows. Hazard zone 5 is on the S flank of Kīlauea, protected topographically (from Kīlauea flows) by N-facing normal faults of the Ko‘ae fault system. Hazard zones 7 and 8 are on Mauna Kea and therefore also topographically protected from Mauna Loa flows, and hazard zone 9 (not shown in Fig. 5) is all of Kohala.

The relationship between our effective effusion-rate-based inundation map and the hazard zone map highlights that our non-probabilistic results are not meant to be used as forecasts of future inundation. Instead, they can be used in more of a scenario-planning mode. In other words, the eventual path and length of a channel-fed flow with a particular effective effusion rate could be determined either prior to, or after the initiation of, an actual eruption. Importantly, if the results we present here are to be useful once an eruption has started, there needs to be a way to relate instantaneous initial effusion rates measured early during an eruption to effective effusion rates that will give an idea of eventual flow length. We note that the effective effusion rate for the combined Flows 1 and 1A of the 1984 eruption was approximately half of the initial effusion rate from the ~2,900-m vents. In practice, once it is evident that a particular location will be the source for a major lava flow, it would be prudent to plot a range of probable channel-fed flow paths and lengths for a range of effective effusion rates. Within a day or two after an eruption starts, more precise estimates of eventual flow lengths would be possible once better estimates of the initial effusion rate were made. Obviously, however, more study is required regarding the relationship between initial and effective effusion rates.

It is critical to note that our modeled results for tube-fed flows are not consistent with actual flows. For example, the tube-fed pāhoehoe portion of the 1859 flow reached the coast south of ‘Anaeho‘omalu with an es-

sentially constant effusion rate of ~5 m^3 s^{-1}, and the tube-fed pāhoehoe portion of the 1880–81 flow reached the outskirts of Hilo at a similar, ~constant effusion rate (Rowland and Walker 1990). This compares, as noted above, to the inability of our modeled 100% crusted flow to reach these distances even with an effusion rate of 10 m^3 s^{-1}. The lack of agreement with our modeled results is due to the fact that a thin moving crust, even if it covers 100% of a channel, is not as efficient a thermal insulator as a thick static lava tube roof. Indeed, the thermal insulation of a mechanically stable tube is sufficient for tube-fed flows to be volume limited rather than cooling limited.

Conclusions

We have characterized the areas of Mauna Loa that can expect to be inundated by channelized lava flows having a range of effective effusion rates. We define the effective effusion rate as that corresponding to creation of ~90% of a flow's length and note that in the 1984 case this was ~twice the mean effusion rate and ~half of the initial effusion rate. Contours of minimum flow length for each effective effusion rate correspond in some instances to previously published lava flow hazard zones determined from inundation interval. Elsewhere the correspondence is poor, mainly because our modeling is non-probabilistic in that it does not take recent eruption location patterns into account.

Nevertheless, our results also point out that topography alone cannot be used to derive potential inundation by channel-fed flows. For example, Hilo turns out to be relatively safe from all but the highest effective-effusion-rate channel-fed flows, especially if the recent lack of eruptions from elevations <2,500 m on the NE rift zone continues. Instead, Hilo is more likely to be threatened by tube-fed pāhoehoe flows. The SW rift zone threatens a considerable portion of ever-more-populated SW flanks, even from channel-fed flows with low to moderate effective effusion rates.

Acknowledgements A thoughtful review by Jim Kauahikaua improved this paper considerably, and we dedicate this work in honor of Jim becoming Scientist in Charge at the Hawaiian Volcano Observatory. Comments by Julie Donnelly-Nolan were also very helpful. This work was funded by NASA Grant no. NAG5-10909 from the Mars Data Analysis Program. This is SOEST Publication no. 6492 and HIGP Contribution no. 1351

Minor modifications to FLOWGO

A few modifications were made to the original version of FLOWGO to improve its ability to model aspects of channelized flows. First, the original version of the program included a term for conductive heat loss into the flow base but inadvertently left out such heat loss to the levees. At the vent, where without independent constraint on channel dimensions we set depth and width equal, conductive heat loss to the levees is twice that to the base. Making the change to include levee heat loss has very little effect on overall flow length when compared to the Mauna Loa, Kīlauea, and Etna test cases because along most of the flow, width is considerably greater than depth. However, its inclusion makes FLOWGO more realistic.

The second minor change has to do with the treatment of yield strength. Jeffreys equation (Jeffreys 1925) as modified by Moore (1987) is the following:

$$V_c = \left[d^2 \rho_{\text{lava}} g \sin\theta / 3\eta_{\text{lava}}\right] \cdot \left\{1 - 3/2(YS_{\text{core}}/\tau_{\text{base}}) + 1/2(YS_{\text{core}}/\tau_{\text{base}})^3\right\} \quad (2)$$

V_c=mean velocity in the channel, d=channel depth, ρ_{lava}=lava viscosity, g=gravity, θ=underlying slope, η_{lava}=lava viscosity, YS_{core}=lava yield strength, and τ_{base}=the shear stress at the base of the flow. The portion of Eq. 2 in square brackets is the Newtonian part and that in the curly brackets is the non-Newtonian part. Note that if $YS_{\text{core}}=0$, the non-Newtonian part becomes unity.

τ_{base} is a limiting value in the sense that as long as the flow core is more fluid than the shear stress required to deform lava at the flow base ($YS_{\text{core}}<\tau_{\text{base}}$), lava will flow. As soon as $YS_{\text{core}}=\tau_{\text{base}}$ (due to cooling of the flow core), then the internal strength of the lava will be greater than the stress driving deformation at its base, and flow will stop (the value in the curly brackets becomes zero).

Originally, FLOWGO determined τ_{base} from the following:

$$\tau_{\text{base}} = \rho_{\text{lava}} g d \sin\theta \quad (3)$$

Although post-eruption yield strength is commonly determined from measuring the dimensions of a flow that has come to rest on a given slope (e.g. Hulme 1974), there is no physical reason why during an eruption the yield strength of flowing lava should be a function of the underlying slope. Additionally, inspection of Eq. 3 shows that as the underlying slope approaches zero, τ_{base} approaches zero. This causes the non-Newtonian portion of Eq. 2 to become negative and a modeled flow would stop purely due to the underlying slope, even if it has cooled only slightly.

There is another method to calculate τ_{base} that is temperature and crystallinity dependent and slope independent (Dragoni 1989; Pinkerton and Stevenson 1992):

$$\tau_{\text{base}} = \left\{6500\phi_{\text{base}}^{2.85}\right\} + b\left\{\exp\left[c\left(T_{\text{erupt}} - T_{\text{base}}\right) - 1\right]\right\} \quad (4)$$

Here, ϕ_{base}=the mass fraction of crystals in the flow base, b and c are constants that have values of 10^{-2} Pa and 0.08 K^{-1}, respectively (Dragoni 1989), T_{erupt}=the eruption temperature, and T_{base}=the temperature of the flow base. Because the temperature difference term (T_{erupt}–T_{base}) is on the order of 400°C, the exponential term becomes very large. YS_{core} is derived from a similar formula (Dragoni 1989; Pinkerton and Stevenson 1992):

$$YS_{\text{core}} = \left\{6500\phi_{\text{core}}^{2.85}\right\} + b\left\{\exp\left[c\left(T_{\text{erupt}} - T_{\text{core}}\right) - 1\right]\right\} \quad (5)$$

Here ϕ_{core}=the mass fraction of crystals in the flow core (which is temperature-dependent and calculated by FLOWGO at each increment downflow). Importantly, the temperature difference (T_{erupt}–T_{core}) is zero at the vent and increases only slightly down flow, meaning that the exponential term here is considerably less than it is for τ_{base} (Eq. 4). Because of this difference in the exponential terms, the quantity $YS_{\text{core}}/\tau_{\text{base}}$ in Eq. 2 is always extremely small and the resulting flow is essentially Newtonian.

Additional consideration of a channelized flow indicates that it isn't the shear stress at the base of the flow that is critical. Instead, it is the shear stress at the base of the channel. Eq. 4 can therefore be modified to:

$$\tau_{\text{base-of-channel}} = \left\{6500\phi_{\text{base-of-channel}}^{2.85}\right\} + b\left\{\exp\left[c\left(T_{\text{erupt}} - T_{\text{base-of-channel}}\right) - 1\right]\right\} \quad (6)$$

The difference between the eruption temperature and that at the base of the channel (T_{erupt}–$T_{\text{base-of-channel}}$) is much closer to that between the eruption temperature and the flow core temperature (T_{erupt}–T_{core}) and therefore so are the exponents associated with these terms. The replacement of $YS_{\text{core}}/\tau_{\text{base}}$ (Eq. 2) with $YS_{\text{core}}/\tau_{\text{base-of-channel}}$ (Eq. 1) means that the yield strength portion of the velocity equation is no longer negligible. Additionally, the yield strength portion of the velocity equation is now dependent on temperature and crystallinity (the mass fraction of crystals at the base of the channel, $\varphi_{\text{base-of-channel}}$, is calculated by FLOWGO) and independent of the underlying slope.

In the original FLOWGO model, T_{hot}, the temperature of lava exposed in cracks in the surface crust, was set to always be T_{core}–140°C, based on field measurements at Etna and Kīlauea (e.g. Calvari et al. 1994; Flynn and Mouginis-Mark 1994). However, it seems unlikely that a constant difference in temperature would be maintained as T_{core} decreases downflow. Instead, the difference between T_{core} and T_{hot} (as well as that between T_{core} and $T_{\text{base-of-channel}}$) should decrease as the flow cools. At the vent, the eruption temperature T_{erupt}=1140°C, the solidus temperature T_{solid}=980°C, T_{core}=T_{erupt}, T_{hot}=T_{core}–140°C, and we consider that $T_{\text{base-of-channel}}$=$T_{\text{hot}}$. The starting conditions therefore are that T_{hot} and $T_{\text{base-of-channel}}$ have a value of T_{core}–0.875(T_{core}–T_{solid}). The final minor FLOWGO change was to maintain this relative temperature spacing. This has the added benefit of preventing both T_{hot} and $T_{\text{base-of-channel}}$ from reaching values less than T_{solid}.

References

Brigham WT (1909) The volcanoes of Kilauea and Mauna Loa. Mem of the Bernice Pauahi Bishop Museum of Polynesian Ethnology and Natural History 2, no. 4, 222 pp

Buchanan-Banks JM (1993) Geologic map of the Hilo 7 1/2' quadrangle, Hawai'i. US Geol Surv Map I-2274

Calvari S, Coltelli M, Neri M, Pompilio M, Scribano V (1994) The 1991-1993 Etna eruption: chronology and lava flow-field evolution. Acta Vulcanol 4:1–14

Diamond J (1999) Guns, germs, and steel. WW Norton & Co, Inc, New York, 457 pp

Dragoni MA (1989) A dynamical model of lava flows cooling by radiation. Bull Volcanol 51:88–95

Easton RM (1987) Stratigraphy of Kilauea Volcano. US Geol Surv Prof Pap 1350:243–260

Farr T, Evans D, Zebker H, Harding D, Bufton J, Dixon T, Vetrella S, Gesch D (1995) Mission in the works promises precise global topographic data. EOS Trans AGU 76:225–229

Felpeto A, Araña V, Ortiz R, Astiz M, García A (2001) Assessment and modelling of a lava flow hazard on Lanzarote (Canary Islands). Natural Hazards 23:247–257

Finch RH, Macdonald GA (1950) The June 1950 eruption of Mauna Loa, Part I. Volcano Lett 508:1–12

Flynn LP, Mouginis-Mark PJ (1994) Temperature of an active lava channel from spectral measurements, Kilauea Volcano, Hawai'i. Bull Volcanol 56:297–301

Glaze LS, Baloga SM (2003) DEM flow path prediction algorithm for geologic mass movements. Environ Eng Geosci 9:225–240

Guest JE, Murray JB (1979) An analysis of hazard from Mount Etna volcano. J Geol Soc Lond 136:347–354

Guest JE, Kilburn RJ, Pinkerton H, Duncan A (1987) The evolution of flow fields: observations of the 1981 and 1983 eruptions of Mount Etna, Sicily. Bull Volcanol 49:527–540

Harris AJL, Murray JB, Aries SE, Davies MA, Flynn LP, Wooster MJ, Wright R, Rothery DA (2000) Effusion rate trends at Etna and Krafla and their implications for eruptive mechanisms. J Volcanol Geotherm Res 102:237–270

Harris AJL, Rowland SK (2001) FLOWGO: a kinematic thermo-rheological model for lava flowing in a channel. Bull Volcanol 63:20–44

Heliker C (1990) Volcanic and Seismic Hazards on the Island of Hawai'i. US Geol Surv General Interest Publ 49 pp

Heliker C, Ulrich GE, Margriter SC, Hoffmann JP (2001) Maps showing the development of the Pu'u 'Ō'ō - Kūpaianaha flow field, June 1984-February 1987, Kīlauea Volcano, Hawai'i. US Geol Surv Geol Investig Ser I-2685

Heliker C, Mattox TN (2003) The first two decades of the Pu'u 'Ō'ō-Kūpaianaha eruption: chronology and selected bibliography. US Geol Surv Prof Pap 1676:1–27

Hulme G (1974) The interpretation of lava flow morphology. Geophys J R Astro Soc 39:361–383

Imhoff M, Story M, Vermillion C, Khan F, Polcyn F (1986) Forest canopy characterization and vegetation penetration assessment with space-borne radar. IEEE Trans Geosci Remote Sens 24:535–542

Jeffreys H (1925) The flow of water in an inclined channel of rectangular section. Phil Mag 49:793–807

Kauahikaua J, Margriter S, Lockwood, Trusdell F (1995) Applications of GIS to the estimation of lava flow hazards on Mauna Loa Volcano, Hawai'i. AGU Geophys Monogr 92:315–325

Kilburn CRJ, Lopes RMC (1988) The growth of aa lava flow fields on Mount Etna, Sicily. J Geophys Res 93 (B12):14,759–14,772

Lipman PW, Swenson A (1984) Generalized geologic map of the southwest rift zone of Mauna Loa Volcano, Hawai'i. US Geol Surv Misc Investig Map I-1323

Lipman PW, Banks NG, Rhodes JM (1985) Gas-release induced crystallization of 1984 Mauna Loa magma, Hawai'i, and effects on lava rheology. Nature 317:604–607

Lipman PW, Banks NG (1987) Aa flow dynamics. US Geol Surv Prof Pap 1350:1527–1567

Lockwood JP, Lipman PW (1987) Holocene eruptive history of Mauna Loa Volcano. US Geol Surv Prof Pap 1350:509–535
Lockwood JP, Dvorak JJ, English TT, Koyanagi RY, Okamura AT, Summers ML, Tanigawa WR (1987) Mauna Loa 1974-1984: a decade of intrusive and extrusive activity. US Geol Surv Prof Pap 1350:537–570
Lockwood JP, Lipman PW, Petersen LD, Warshaur FR (1988) Generalized ages of surface lava flows of Mauna Loa volcano, Hawai'i. US Geol Surv Misc Invest Map I-1908
Lockwood JP (1995) Mauna Loa eruptive history - the preliminary radiocarbon record. AGU Geophys Monogr 92:81–94
Macdonald GA (1943) The 1942 eruption of Mauna Loa, Hawai'i. Am J Sci 241:241–256
Macdonald GA, Finch RH (1950) The June 1950 eruption of Mauna Loa, Part II. Volcano Lett 509:1–6
Macdonald GA (1954) Activity of Hawaiian volcanoes during the years 1940–1950. Bull Volcanol 15:119–179
Macdonald GA, Abbot AT, Peterson FL (1983) Volcanoes in the Sea: the geology of Hawai'i. Univ Hawai'i Press, Honolulu, 517 pp
Moore HJ (1987) Preliminary estimates of the rheological properties of 1984 Mauna Loa lava. US Geol Surv Prof Pap 1350:1569–1588
Moore JG, Fornari DJ, Clague DA (1985) Basalts from the 1877 submarine eruption of Mauna Loa, Hawai'i: new data on the variation of palagonitization rate with temperature. US Geol Surv Bull 1663:11 pp
Mouginis-Mark PJ, Gradie J, Hagler C, Craig B (2003) Production of cloud-free satellite image maps of hazardous volcanoes. Cities on Volcanoes III Abs Vol: 88
Mullineaux DR, Peterson DW, Crandell DR (1987) Volcanic hazards in the Hawaiian Islands. US Geol Surv Prof Pap 1350:599–621
Office of Planning (2003a), State of Hawai'i Dept. of Business Economic Development and Tourism, Data Center Reports and Tables: http://www.hawaii.gov/dbedt/census2k/pltable1.html
Office of Planning (2003b), State of Hawai'i Dept. of Business Economic Development and Tourism, Census Profiles - Hawai'i County website: http://www.hawaii.gov/dbedt/census2k/profile-hawaii/index.html
Pinkerton H, Stevenson RJ (1992) Methods of determining the rheological properties of magmas at sub-liquidus temperature. J Volcanol Geotherm Res 53:47–66
Pinkerton H, Wilson L (1994) Factors controlling the lengths of channel-fed lava flows. Bull Volcanol 56:108–120
Rowland SK, Walker GPL (1990) Pahoehoe and aa in Hawai'i: volumetric flow rate controls the lava structure. Bull Volcanol 52:615–628
Rowland SK, Garbeil H (2000) Slopes of oceanic basalt volcanoes. AGU Geophys Monogr 116:223–247
Rowland SK, Harris AJL, Wooster MJ, Amelung F, Garbeil H, Wilson L, Mouginis-Mark PJ (2003) Volumetric characteristics of lava flows from interferometric radar and multispectral satellite data: the 1995 Fernandina and 1998 Cerro Azul eruptions in the western Galápagos. Bull Volcanol 65:311–330
Trusdell FA (1995) Lava flow hazards and risk assessment on Mauna Loa Volcano, Hawai'i. AGU Geophys Monogr 92:327–336
Wadge G (1981) The variation of magma discharge during basaltic eruptions. J Volcanol Geotherm Res 11:139–168
Wadge G, Young PAV, McKendrick IJ (1994) Mapping lava flow hazards using computer simulation. J Geophys Res 99(B1): 489–504
Walker GPL (1972) Compound and simple lava flows. Bull Volcanol 35:579–590
Walker GPL (1974) Volcanic hazards and the prediction of volcanic eruptions. In: The prediction of geological hazards, Geol Soc Lond Misc Paper 3:23–41
Wolfe EW, Neal CA, Banks NG, Duggan TJ (1988) Geologic observations and chronology of eruptive events. US Geol Surv Prof Pap 1463:1–97
Wright TL, Chun JYF, Esposo J, Heliker C, Hodge J, Lockwood JP, Vogt SM (1992) Map showing lava-flow hazard zones, Island of Hawai'i. US Geol Surv Misc Field Studies Map MF-2193
Wright R, Flynn LP, Harris AJL (2001) The evolution of lava flowfields at Mount Etna, 27-28 October 1999, observed by Landsat 7 ETM+. Bull Volcanol 63:1–7
Young PAV, Wadge G (1990) FLOWFRONT: simulation of a lava flow. Comput Geosci 16:1171–1191
Zebker HA, Farr TG, Salazar RP, Dixon TH (1994) Mapping the world's topography using radar interferometry: the TOPSAR mission. IEEE Trans Geosci Remote Sens 82:1744–1786